IEEE Access
Multidisciplinary ⋮ Rapid Review ⋮ Open Access Journal

Received 19 August 2024, accepted 3 September 2024, date of publication 6 September 2024,
date of current version 19 September 2024.

Digital Object Identifier 10.1109/ACCESS.2024.3456038

RESEARCH ARTICLE

A Novel Method to Design Small Wideband Half Mode Cavity Antenna Under Resonances of $TM_{1,1}$ and $TM_{3,1}$ Modes

MOHAMMAD HADI MORADI ARDEKANI[1] **AND SHIMA PASHANGEH**[2]
[1]Department of Electrical Engineering, Faculty of Engineering, Yasouj University, Yasouj 75918-74934, Iran
[2]Department of Materials Engineering, School of Engineering, Yasouj University, Yasouj 75918-74934, Iran

Corresponding author: Mohammad Hadi Moradi Ardekani (m.moradi@yu.ac.ir)

ABSTRACT In this study, we propose a novel method for designing a compact and wideband half-mode cavity antenna (HMCA) that simultaneously radiates in the $TM_{1,1}$ and $TM_{3,1}$ modes. This advancement leverages an intrinsic property of HMCAs that has not been addressed in previously reported research. It is investigated that for a conventional HMCA with proper dimensions, resonant frequencies of $TM_{1,1}$ ($f_{1,1}$) and $TM_{3,1}$ ($f_{3,1}$) modes converge closely, whereas the resonant frequency of $TM_{2,2}$ ($f_{2,2}$) mode shifts out of the range between these two modes. So, unlike conventional methods, a wide frequency bandwidth can be realized without employing any extra components such as shorting pins and slots which add complexity and cost to the design and deteriorate cross polarization. However, since this modes reallocation results in a low input admittance, a stepped probe feed is used for excitation to enhance input reflection coefficient (S_{11}). Consequently, the dual resonance operation achieves a broad frequency bandwidth, characterized by low cross-polarization, a stable radiation pattern, and minimal gain fluctuation. Antenna exhibits more than 21% size reduction compared with the wideband HMCAs proposed in the recently published articles. The proposed HMCA is implemented and tested to verify the design approach.

INDEX TERMS Cross polarization, half mode cavity antenna, resonant modes, small size, wide bandwidth.

I. INTRODUCTION

Ease of fabrication, low weight and simple integration with other components make microstrip patch antennas (MPA) popular for different applications [1], [2]. To reduce dielectric loss and improve efficiency, air substrate is preferred [3]. However, since MPAs are suspended above a metal ground plane, supporting structures are required to boost rigidity and robustness [4]. In addition, traditional MPAs suffer from high side lobes of E-plane radiation pattern [5], [6]. To avoid these extra structures which add complexity and cost to the design and reduce E-plane side lobes, planar inverted-F antennas (PIFAs) can be used. It consists of a quarter-wave patch and a shorting wall to ensure electrical symmetry [7]. Despite its good efficiency, the uniform electric field distribution across the antenna H-plane and the strong field at the non-radiating edges result in significant mutual coupling with nearby components and high cross polarization. Moreover, low gain and narrow frequency bandwidth are two additional intrinsic disadvantages of the conventional PIFA which degrade overall performance of the systems [8]. It has been reported in different literatures that by shorting non-radiating edges of the PIFA, boundary conditions are changed which results in a tighter electric field distribution across the H-plane and consequently mutual coupling is enhanced [7], [9], [10], [11], [12], [13], [14]. This reformed PIFA which is also known as half mode cavity antenna (HMCA) experiences a lower cross polarization (cross-pol) compared with the conventional PIFA. In addition, HMCA resonates at the higher frequency than PIFA with the same size which yields to the higher gain. However, narrow frequency bandwidth is still a real bottleneck for HMCA to be employed in wideband communication systems. Inserting shorting pins and cutting slots are promising approaches to reallocate radiative modes

The associate editor coordinating the review of this manuscript and approving it for publication was Feng Wei.

in the proximity of the each other so as to broaden frequency bandwidth of the planar antennas [15], [16], [17], [18], [19], [20]. Despite usefulness of these methods in term of widening frequency bandwidth, loading extra components results in the field perturbation underneath of the antenna and consequently cross-pol is relatively degraded. Besides, antennas have to be enlarged in length or width in order to be suitable for combining radiative modes which in company with inserting shorting posts or cutting slots, intrinsic properties of the planar antennas such as ease of fabrication, light weight and compact size are destroyed. For instance, a HMCA with six shorting pins and two slots was proposed in [21] to acquire 26.2% bandwidth and -12.3 dB cross-pol. However, gain fluctuation is more than 3 dB over the operating band and patch size is as large as 0.71 λ^2. In [22], the resonant frequency of TM_{11} ($f_{1,1}$) increases by loading six shorting pins beneath an HMCA around the nodal line of the electric field of the $TM_{2,2}$ mode, with minimal impact on the resonant frequency of $TM_{2,2}$($f_{2,2}$). Therefore, two resonant frequencies are combined and a wide frequency bandwidth of 14.7 % is achieved. The patch size and H-plane cross-pol are approximately λ^2 and -13 dB, respectively. Due to their large size, use of these two wide band HMCAs are undesirable for the medical monitoring, sport and security applications. Moreover, contemporary communication systems require increased frequency bandwidth, reduced cross-pol, and a stable radiation pattern throughout the operating band [23], [24].

This paper proposes a compact, wideband HMCA with low cross polarization. It will be demonstrated that the resonant frequencies of all radiative mode of the conventional HMCA can be controlled by both length and width of the antenna. Since this dependency on the antenna size is different for each mode, $f_{1,1}$ and resonant frequencies of $TM_{3,1}$ mode ($f_{3,1}$) are reallocated in the proximity of each other by adjusting patch size. In this case $f_{2,2}$ is suppressed in the frequency range between $f_{1,1}$ and $f_{3,1}$ and antenna operates under dual resonances without employing any extra components. However, since input admittance is low for input reflection coefficient (S_{11}) lower than -10 dB, a stepped probe feed is applied to excite the proposed HMCA. Achieving a broad frequency coverage of 37.5% (1.97-2.88 GHz) for S_{11} <-10 dB with consistent radiation pattern stability has been successfully achieved. Patch size is around 0.56λ^2 which exhibits 21% and 44% size reduction compared with the recently presented wide band HMCAs in [21] and [22], respectively. Gain fluctuation and cross-pol are respectively lower than 0.7 dB and 20 dB over the operating band. To validate the proposed antenna, a prototype was fabricated and tested, showing strong agreement between measured and simulated results. The proposed structure's wide bandwidth, compact size, straightforward design, and consistent radiation pattern render it versatile for a range of applications.

The paper is structured as follows: Section II discusses the design of the proposed wideband patch antenna, including simulation and theoretical results. It also includes an evolutionary and parametric study to elucidate the operational principles of the structure. Section III presents the implementation and measurement of a prototype, while Section IV provides the conclusion.

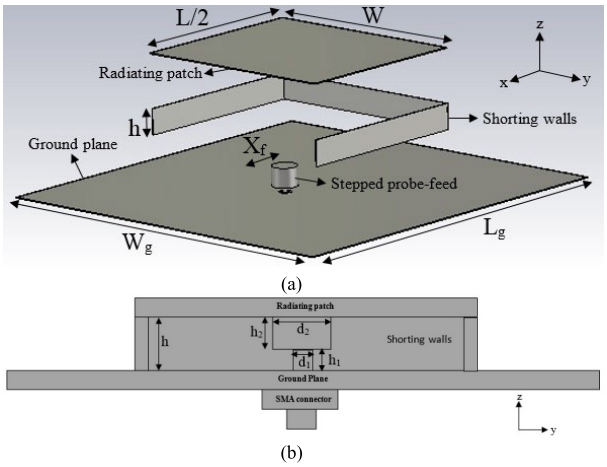

FIGURE 1. The geometry of the proposed structure. (a) 3D view of the antenna. (b) Schematic of the antenna (cross-sectional view).

TABLE 1. Optimized dimensions of the proposed structure.

Parameters	L	W	L_g	W_g	X_f
Values(mm)	172.5	99.75	180	180	32.25
Parameters	h	h_1	d_1	h_2	d_2
Values(mm)	12	3	1.72	9	12

II. ANTENNA DESIGN AND ANALYSIS

A. ANTENNA GEOMETRY

Fig. 1 illustrates the three-dimensional (3D) geometry and schematic of the proposed wideband HMCA, showcasing its key parameters. The structure comprises a rectangular radiating patch with dimensions L/2 (length) and W (width), elevated at a height H above a ground plane sized $L_g \times W_g$. Vertical connecting walls ground three edges of the radiative patch to the ground plane. The antenna is fed at a distance X_f from the radiating aperture along the x-axis direction. Herein, a two-step probe-feed with heights and diameters of $h_1 \times d_1$ and $h_2 \times d_2$ is employed to boost input impedance matching. The optimized dimensions of the proposed structure are detailed in Table 1. Simulation tasks utilized the commercial high-frequency structure simulator CST, employing the finite integration method.

B. WORKING PRINCIPLE

The primary objective in this section is to adjust the resonant frequencies of the $TM_{1,1}$ and $TM_{3,1}$ modes to be in close proximity while suppressing other modes within this frequency range. This approach results in a wide frequency bandwidth with a stable radiation pattern and consistent polarization under dual resonance operation.

At the beginning, according to the well-known cavity model [3], working mechanism of the conventional HMCA is studied. Although this model was initially applied to describe

internal field distribution of the MPA, it can be modified to analyze other cavities with different boundary condition as well. The development process of the proposed wideband HMCA is depicted in Fig. 2, with the corresponding simulation results shown in Fig. 3. A rectangular cavity surrounded by perfect electric conductors with size of L×W×h is depicted in fig. 2(a). Given that the height h is much smaller than the wavelength (h$\ll \lambda$), the fields can be approximated as constant along this dimension ($\frac{\partial}{\partial z} = 0$). Moreover, due to the minimal height of the substrate, the electric field is oriented perpendicularly to the top patch, leading to the exclusive consideration of TM^z modes within the cavity. Under these specific conditions, the field distribution for TM^z modes in this rectangular cuboidal cavity and their associated resonant frequencies can be derived using the cavity model through the vector potential method. In this scenario, the vector potential A_z must satisfy the homogeneous wave equation, expressed as:

$$\nabla^2 A_z + \left(\frac{2\pi f_r}{c}\right)^2 A_z = 0 \tag{1}$$

where f_r and c denote the cavity's resonant frequency and the speed of light, respectively. By applying the method of separation of variables, the solution to (1) can be derived as follows:

$$\begin{aligned} A_z = &[C_1 \cos(\beta_x x) + D_1 \sin(\beta_x x)] \\ &\times \left[C_2 \cos\left(\beta_y y\right) + D_2 \sin\left(\beta_y y\right)\right] \end{aligned} \tag{2}$$

In this expression, β_x and β_y represent the wavenumbers in the x and y directions, respectively. These wavenumbers are determined by imposing the relevant boundary conditions and are governed by the relation:

$$\sqrt{\beta_x^2 + \beta_y^2} = \frac{2\pi f_r}{c}. \tag{3}$$

Assuming no variation along the z-axis, the electric and magnetic fields within the cavity can be expressed in terms of A_z as follows [25]:

$$\begin{aligned} E_x &\propto \frac{\partial A_z}{\partial x \partial z} = 0 \\ E_y &\propto \frac{\partial A_z}{\partial y \partial z} = 0 \\ E_z &\propto A_z \\ H_x &\propto \frac{\partial A_z}{\partial y} \\ H_y &\propto \frac{\partial A_z}{\partial x} \\ H_z &= 0 \end{aligned} \tag{4}$$

Given that the tangential electric field must vanish on a perfect electric conductor, E_z, or equivalently A_z as described by Equation (4), must be zero at the four surrounding walls located at $x = 0$, $x = L$, $y = 0$, and $y = W$. Applying these boundary conditions, we find that:

$$C_1 = C_2 = 0$$

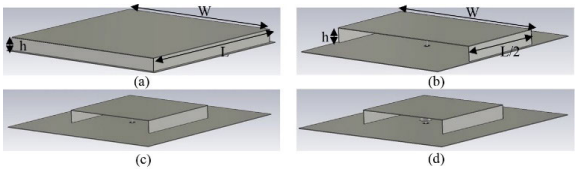

FIGURE 2. The evolution process of the proposed structure. (a) Conventional square cavity (L=W). (b) Square HMCA (L=W) with simple probe excitation. (c) HMCA with reduced width and simple probe excitation. (d) HMCA with reduced width and stepped probe excitation.

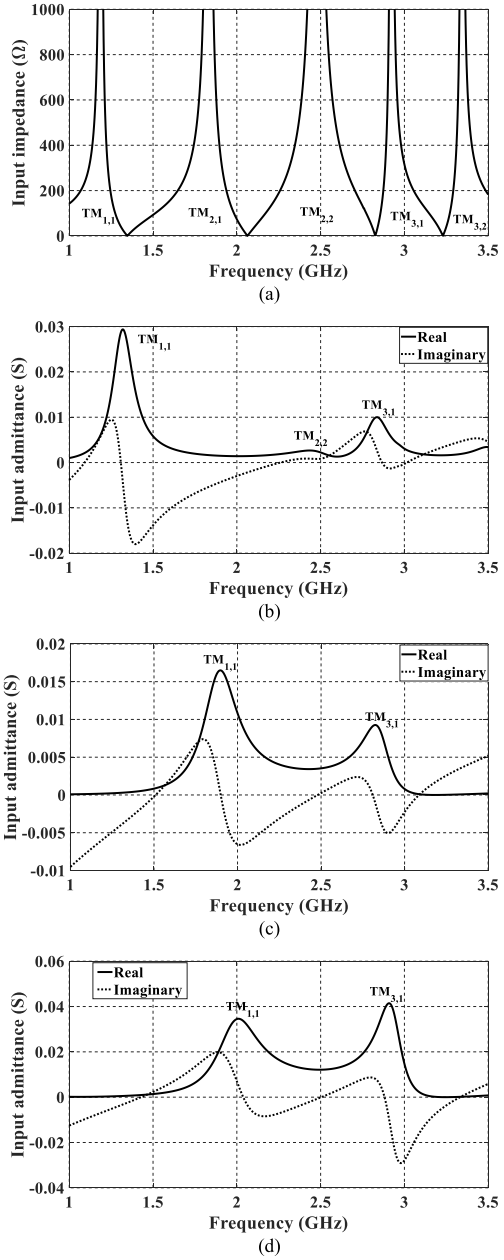

FIGURE 3. Simulated input performance of the structures in fig. 2.

$$\begin{aligned} \beta_x &= \frac{m\pi}{L} \\ \beta_y &= \frac{n\pi}{W} \end{aligned} \tag{5}$$

where m and n are integers taking values 1, 2, 3, and so on.

With these conditions, the resonant frequencies and field configurations of TM^z modes can be determined using Equations (3) and (4) as follows:

$$E_z \propto \sin\left(\frac{m\pi}{L}x\right)\sin\left(\frac{n\pi}{W}y\right) \tag{6}$$

$$H_x \propto \sin\left(\frac{m\pi}{L}x\right)\cos\left(\frac{n\pi}{W}y\right) \tag{7}$$

$$H_y \propto \cos\left(\frac{m\pi}{L}x\right)\sin\left(\frac{n\pi}{W}y\right) \tag{8}$$

$$f_{r_{m,n}} = \frac{c}{2}\sqrt{\left(\frac{m}{L}\right)^2 + \left(\frac{n}{W}\right)^2} \tag{9}$$

So, feeding in an appropriate position can excite all even- and odd-order modes within the cavity. Fig. 3(a) shows the simulated frequency response of the input impedance magnitude for a square cavity, fed by a simple coaxial probe along the x-direction. All dimensions are as specified in Table 1, except for W, which is set to 172.5 mm. The simulated result shows that $TM_{1,1}$ and $TM_{3,1}$ resonate at 1.24 and 2.7 GHz, respectively, which are far away from each other. Moreover, redundant resonant frequencies, i.e. $f_{2,1}$ and $f_{2,2}$, which are in the frequency range between these dual modes, need to be suppressed. It should be noted that the resonant frequency values show a close correspondence with those predicted by (9). Equations (6)-(8) clearly indicate that the central planes of the cavity can be treated as perfect magnetic walls for even-order modes and perfect electric walls for odd-order modes. Therefore, introducing an open aperture as equivalent magnetic symmetry at the middle of the cavity leads to the odd-order modes removal and a HMCA is built up (fig. 2(b)). In this case, even-order modes, i.e., $TM_{1,1}$, $TM_{3,1}$ and $TM_{2,2}$, with radiation peaks in the broadside direction are only supported. The simulated square cavity is halved along the x-direction and its corresponding simulated input admittance confirm the suppression of all odd-order modes as demonstrated in fig.3(b).

It can be noticed that $f_{1,1}$, $f_{2,2}$ and $f_{3,1}$ are approximately unchanged. The small change of resonant frequencies of even-order modes can be attributed to the fringing field at the radiating edge and inductive loading of the coaxial probe. Since radiating slot can be modeled by a parallel equivalent admittance, the frequency response of the input admittance is preferred for planar antennas [3].

The next step is to suppress $TM_{2,2}$ mode in the frequency range between $TM_{1,1}$ and $TM_{3,1}$ modes and move these dual modes close to each other for combination. In contrast with MPA, all resonant frequencies of HMCA are simultaneously related to the both length and width of the cavity and these relations are different for each mode. So, changing aspect ratio of the cavity ($\frac{W}{L}$) influences all the radiative resonant frequencies in different way.

Firstly, the condition of $f_{2,2}f_{3,1}$ must hold in order to suppress $TM_{2,2}$ mode in the frequency range between $f_{1,1}$ and $f_{3,1}$. According to the (9), antenna dimensions are thus

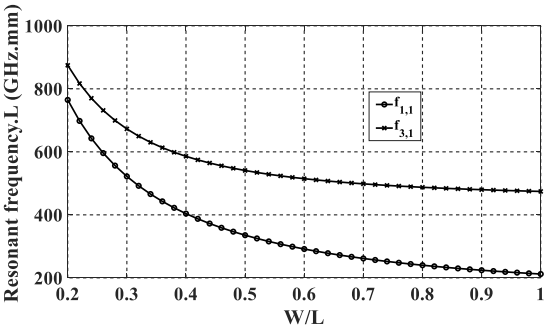

FIGURE 4. Resonant frequencies of the cavity versus cavity aspect ratio.

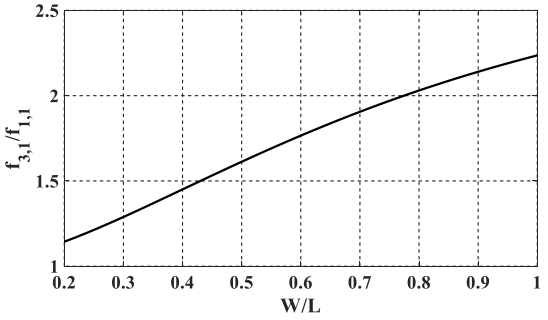

FIGURE 5. Frequency ratio versus cavity aspect ratio.

required to satisfy

$$\sqrt{\left(\frac{2}{L}\right)^2 + \left(\frac{2}{W}\right)^2} > \sqrt{\left(\frac{3}{L}\right)^2 + \left(\frac{1}{W}\right)^2} \tag{10}$$

After simplification, the following relationship for the cavity dimensions is derived:

$$\frac{W}{L} < 0.77 \tag{11}$$

Therefore, by ensuring that the patch width W is less than 0.77 times the patch length L, all undesired modes are shifted out of the frequency range between the $TM_{1,1}$ and $TM_{3,1}$ modes.

Secondly, to broaden the frequency bandwidth by reallocating the $TM_{1,1}$ and $TM_{3,1}$ modes, $f_{1,1}$ and $f_{3,1}$ should be brought closer together. According to equation (9), the following expressions are obtained:

$$f_{1,1}L = 0.15\sqrt{1 + \frac{1}{\left(\frac{W}{L}\right)^2}}(GHz.mm)$$

$$f_{3,1}L = 0.45\sqrt{1 + \frac{1}{\left(\frac{3W}{L}\right)^2}}(GHz.mm) \tag{12}$$

Fig. 4 illustrates the plots of $f_{1,1}L$ and $f_{3,1}L$ versus the aspect ratio $\frac{W}{L}$. As anticipated, both resonant frequencies increase as $\frac{W}{L}$ decreases, with $f_{1,1}$ rising more rapidly than $f_{3,1}$, facilitating the reallocation. To enable this reallocation, the frequency ratio $\frac{f_{3,1}}{f_{1,1}}$ must be reduced. From equation (9), $\frac{f_{3,1}}{f_{1,1}}$ can be

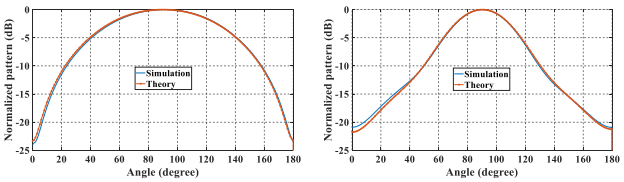

FIGURE 6. Simulated and theoretical far-field pattern in h-plane. (a) $TM_{1,1}$ mode. (b) $TM_{3,1}$ mode.

expressed as:

$$\frac{f_{3,1}}{f_{1,1}} = \sqrt{\frac{1+\left(\frac{3W}{L}\right)^2}{1+\left(\frac{W}{L}\right)^2}} \tag{13}$$

For further clarification, fig. 5 shows the frequency ratio $\frac{f_{3,1}}{f_{1,1}}$ as a function of the aspect ratio $\frac{W}{L}$. It is observed that a decrease in the aspect ratio leads to a reduction in the frequency ratio.

The HMCA with dimensions listed in Table 1 ($\frac{W}{L} = 0.58$) is excited by a simple probe feed (fig. 2(c)) and its corresponding simulated input admittance is plotted in fig. 3(c). It is evident that $TM_{1,1}$ and $TM_{3,1}$ modes merge effectively with a frequency ratio of approximately 1.5, aligning well with the theoretical results shown in fig. 5. The small discrepancy is due to the fringing field ignorance in the theoretical formula. In addition, since aspect ratio is lower than 0.77, $TM_{2,2}$ mode is automatically suppressed. Therefore, in contrast with previous works, two radiative modes of a planar antenna are combined without employing any shorting pins and slots. This achievement is due to the intrinsic property of the HMCA which has not yet been considered in the previously published literatures. However, antenna exhibits a low input admittance over the frequency bandwidth.

Prior to enhancing the antenna's input matching, the radiation characteristics of these dual modes are analyzed. It is established that the HMCA primarily radiates from the aperture at the end of the structure. Assuming an infinite ground plane, this aperture can be modeled as an equivalent magnetic current, represented by, $\vec{M} = -2\hat{n} \times \vec{E}_t$, where $\hat{n}$ is the unit vector normal to the aperture and $\vec{E}_t$ is tangential electric field at the aperture. Consequently, based on Equation (6), the far-field radiation pattern of the antenna in the upper half-space for the $TM_{1,0}$ and $TM_{3,1}$ modes can be

derived using the following magnetic currents:

$$\vec{M}_{1,1} \propto \hat{y} \sin\left(\frac{\pi}{W}y\right)$$
$$\vec{M}_{3,1} \propto \hat{y} \sin\left(\frac{3\pi}{W}y\right) \tag{14}$$

By employing the auxiliary vector potential method as described in [25], the far-field radiation patterns for these equivalent magnetic current sources can be determined. Given that for a single magnetic current on an infinite ground plane, the radiation pattern in the E-plane is uniform, only the H-plane far-field patterns are considered [21]. Theoretical

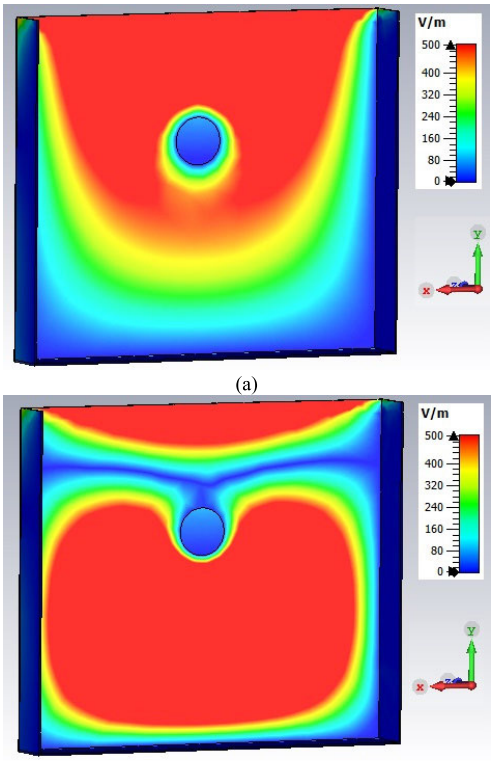

FIGURE 7. Simulated electric-field distribution beneath the radiating patch. (a) $f_{1,1} = 2$ GHz. (b) $f_{3,1} = 2.9$ GHz.

and simulated far-field patterns in the H-plane are shown in Fig. 6. The results demonstrate a strong agreement between theoretical predictions and simulations, with both modes exhibiting a unidirectional radiation pattern. So, the antenna performs well in terms of frequency bandwidth and radiation characteristics.

Finally, in place of a probe with constant diameter, herein the cross section of the probe feed is varied so as to improve input matching. Indeed, a two-step probe with different diameters and heights is used to excite the proposed HMCA as depicted in fig. 2(d). The heights and diameters of the steps are optimized and corresponding simulated input admittance in fig. 3(d), demonstrating suitable values for S_{11} <-10 dB across the frequency band from 1.98 to 2.88 GHz. Fig. 7 illustrates the magnitude of the electric-field distribution beneath the radiating patch of the proposed HMCA at 2 GHz and 2.9 GHz. The nulls in the electric-field intensity at lower resonance primarily concentrate around the shorting edges due to $TM_{1,1}$ mode excitation. While an additional null is observed along the length at high frequency (2.9 GHz), the electric-field configuration is unchanged along the width of the patch implying that $TM_{3,1}$ mode is excited.

C. PARAMETRIC STUDY

It can be easily inferred from described working principle that antenna aspect ratio and stepped probe feed have the most significant influences on the resonant frequencies. A parametric study is conducted here to explore how dimensions of

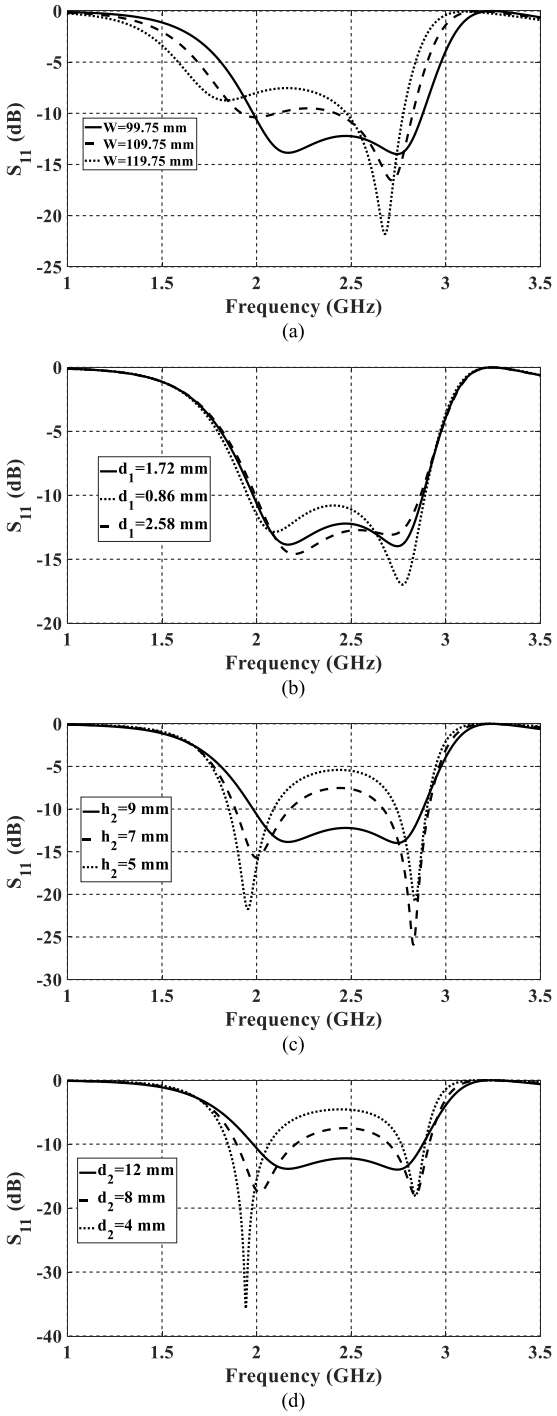

FIGURE 8. Parametric study of the proposed structure. (a) W. (b) d_1. (c) h_2. (d) d_2.

the proposed structure impact antenna performance. Aforementioned parameters are individually studied while others are kept as optimum values according to the Table 1.

Initially, patch width W is selected and its impact on the resonance modes are examined. Fig. 8(a) depicts the frequency response of the simulated input reflection coefficient for various values of W. It is noted that two resonant frequencies go down as W increases. However, frequency displacement for lower resonance is faster and consequently frequency ratio is enlarged which confirms the design principle.

Next, the simulated S_{11} under different radius of the first probe step d_1 is displayed in fig. 8(b). It should be noted that the output shield of the coaxial probe is adjusted for each individual d_1 to form a 50 Ω input SMA connector. The results indicate that S_{11} is approximately irrelevant to the d_1 as long as a 50 Ω connector is applied to feed antenna. So, it can be concluded that the only difference of the proposed structure with conventional one is employing an additional cylinder with radius d_2 and height h_2 attached to the antenna which result in a simple structure without any complexities in the fabrication processes.

Then, h_2 is studied and the corresponding simulated S_{11} in fig. 8(c) showing frequency ratio increases as h_2 decreases and subsequently input matching deteriorates. The same outcome for d_2 is observed in fig. 8(d) which evinces the importance of the stepped probe feed in the proposed structure.

In conclusion, two resonant frequencies contributed by $TM_{1,1}$ and $TM_{3,1}$ modes are reallocated in a close proximity to widen frequency bandwidth to around 37%. The design principles and parametric study offer a clear understanding of the antenna's operational characteristics.

III. EXPERIMENTAL VERIFICATION

A prototype of the structure depicted in fig. 1, with dimensions listed in Table 1, is fabricated and tested to validate the design procedure, as illustrated in fig. 9. A 0.25 mm thick steel sheet, electroplated with tin and silver, was used for antenna fabrication. As depicted, besides soldering, a screw was employed to bolster the connection between the stepped probe feed and the antenna, enhancing structural integrity.

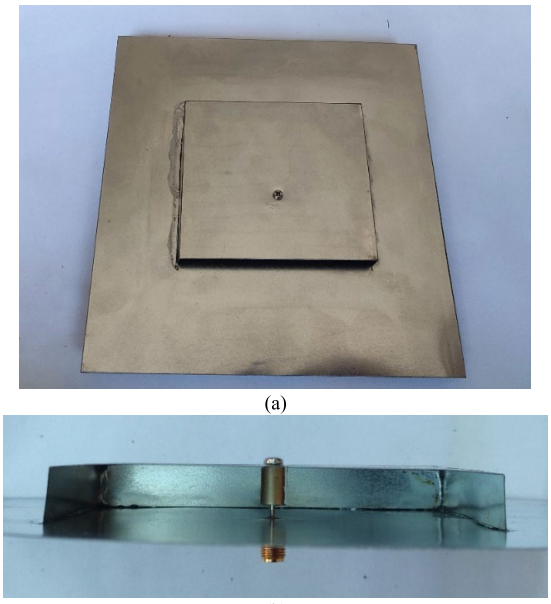

FIGURE 9. Photographs of fabricated structure. (a) Top view. (b) Inside view.

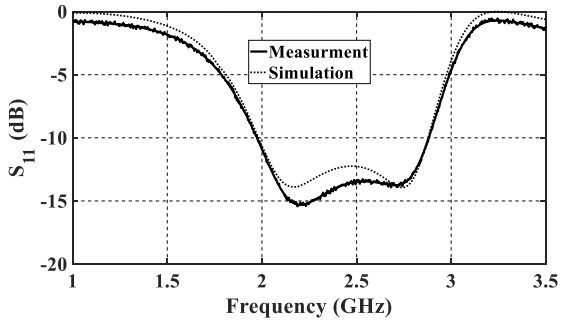

FIGURE 10. Simulated and measured S_{11} of the proposed wide band antenna versus frequency.

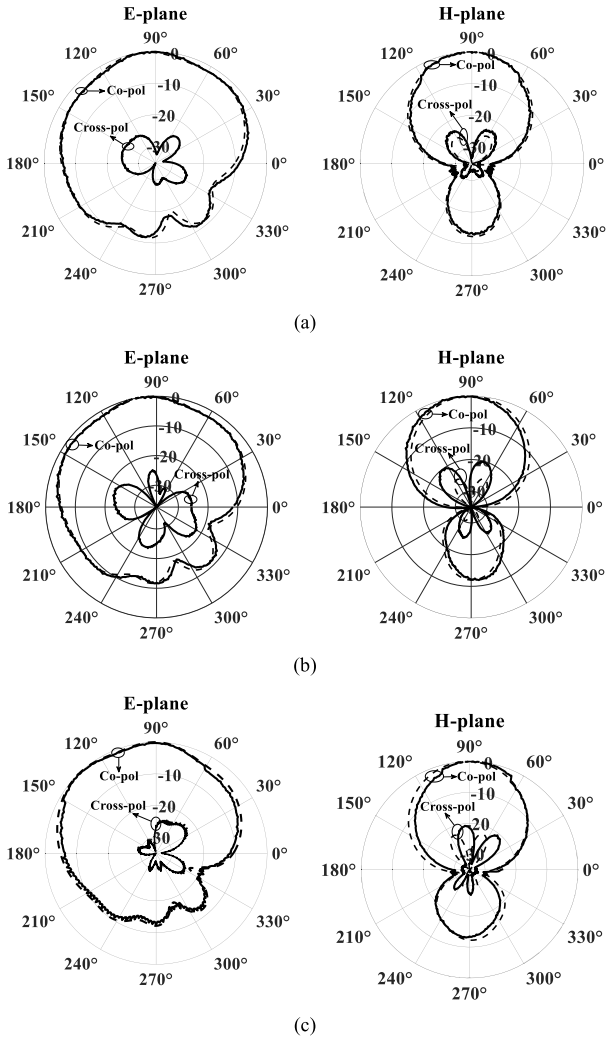

FIGURE 11. Simulated (…) and measured (-) normalized radiation pattern of proposed wide band antenna in E- and H-planes. (a) 2.2 GHz. (b) 2.425 GHz. (c) 2.6 GHz.

Input reflection coefficient measured by Agilent vector network analyzer alongside simulated one are demonstrated in fig. 10. The results show a strong agreement between experimental measurements and simulations. Two in-band attenuation poles are observed at 2.2 GHz and 2.6 GHz, achieving a wide frequency bandwidth of 37.5% from 1.97 GHz to 2.88 GHz. The small variation between measured and simulated results may be attributed to fabrication tolerances. Radiation characteristics of the proposed HMCA are evaluated using an anechoic chamber.

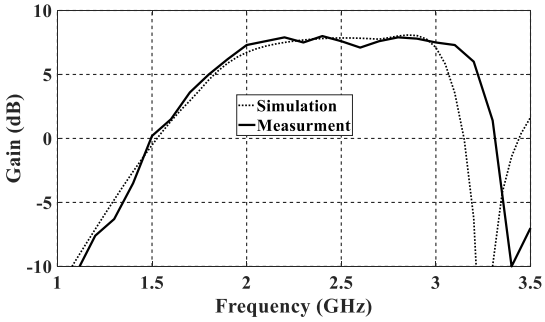

FIGURE 12. Simulated (…) and measured (-) gain of the proposed wide band antenna versus frequency.

Fig. 11 illustrates the simulated and measured radiation patterns at three different frequencies. The measured results are in good agreement with the simulated results, showing stable and unidirectional co-polarization (co-pol) across the frequency bandwidth. The cross-pol in the E-plane and H-plane is below -20 dB.

Fig. 12 shows the simulated and measured peak gain of the proposed HMCA. A stable peak gain with fluctuations of less than 0.7 dB, ranging from 7.3 to 8 dB across the frequency band, is achieved.

Table 2 offers a thorough comparison between the present study and its earlier variants as documented in prior literature, underscoring the advantages of the proposed structure. The structures discussed in [18], [19], and [20] are characterized by significant gain variation or high cross-pol, making them inappropriate for practical applications. In comparison with the findings in [21] and [22], the designed wideband HMCA exhibits a broader frequency bandwidth, reduced cross-polarization, and more consistent gain. Additionally, the antenna area is reduced by approximately 21% and 44% relative to [21] and [22], respectively. These improvements highlight the proposed design's considerable suitability for modern communication systems.

TABLE 2. Performance comparison with previous wideband HMCAs.

Ref.	Patch size (λ^2)	Freq. (GHz)	Fractional Bandwidth	Cross-pol (dB)	Gain (dB)
[18]	0.4	5.34	15.7%	Not given	2.9-7.1
[19]	0.25	2.4	9.1%	<-7.8	Not given
[20]	0.44	2.5	14.9%	<-4.7	4.3-9
[21]	0.71	4.43	26.2%	<-12.3	6.8-10
[22]	1	5.48	14.7%	<-15	9.2-11
This work	0.56	2.425	37.5%	<-20	7.3-8

λ: free space wavelength at the center frequency.

IV. CONCLUSION

A new approach to reallocate radiative $TM_{1,1}$ and $TM_{3,1}$ modes in a conventional HMCA has been presented in this study. The reallocation is accomplished without employing

any extra components such as shorting pins and slots which result in cross-pol degradation, large size and high fabrication cost and complexity. Narrowing the antenna width merges $TM_{1,1}$ and $TM_{3,1}$ modes closely together, while $TM_{2,2}$ is shifted away from intermediate frequency between these two modes. Moreover, a stepped probe feed is used for excitation to enhance input impedance matching. In this case, a small size HMCA with stable radiation pattern and low cross-pol over a wide frequency bandwidth is achieved. The proposed wideband structure, featuring stepped probe excitation and a compact size of $0.56\lambda^2$, is fabricated and tested to validate the design approach. A wide frequency bandwidth with two distinct attenuation poles is achieved. Both E-plane and H-plane cross-polarizations are below -20 dB across the entire frequency bandwidth. Achievable peak gain over the band is higher than 7.3 dB with gain variation lower than 0.7 dB. Hence, the compact HMCA, characterized by its wide frequency bandwidth, minimal cross-polarization, and consistent radiation pattern, holds promise for various applications in modern communication systems.

REFERENCES

[1] J.-S. Row and Y.-Y. Liou, "Broadband short-circuited triangular patch antenna," *IEEE Trans. Antennas Propag.*, vol. 54, no. 7, pp. 2137–2141, Jul. 2006.

[2] K. L. Lau, P. Li, and K. M. Luk, "A wideband and dual-frequency shorted-patch antenna with compact size," in *Proc. IEEE Antennas Propag. Soc. Symp.*, vol. 1, Jun. 2004, pp. 249–252.

[3] C. A. Balanis, *Antenna Theory: Analysis and Design*, 2nd ed., New York, NY, USA: Wiley, 2001.

[4] F. Croq and A. Papiernik, "Large bandwidth aperture-coupled microstrip antenna," *Electron. Lett.*, vol. 26, no. 16, p. 1293, 1990.

[5] N.-W. Liu, L. Zhu, W.-W. Choi, and X. Zhang, "A low-profile aperture-coupled microstrip antenna with enhanced bandwidth under dual resonance," *IEEE Trans. Antennas Propag.*, vol. 65, no. 3, pp. 1055–1062, Mar. 2017.

[6] N.-W. Liu, L. Zhu, and W.-W. Choi, "A differential-fed microstrip patch antenna with bandwidth enhancement under operation of TM_{10} and TM_{30} modes," *IEEE Trans. Antennas Propag.*, vol. 65, no. 4, pp. 1607–1614, Apr. 2017.

[7] F.-X. Liu, T. Kaufmann, Z. Xu, and C. Fumeaux, "Wearable applications of quarter-wave patch and half-mode cavity antennas," *IEEE Antennas Wireless Propag. Lett.*, vol. 14, pp. 1478–1481, 2015.

[8] X. Zhang and L. Zhu, "Gain-enhanced patch antennas with loading of shorting pins," *IEEE Trans. Antennas Propag.*, vol. 64, no. 8, pp. 3310–3318, Aug. 2016.

[9] S. Agneessens and H. Rogier, "Compact half diamond dual-band textile HMSIW on-body antenna," *IEEE Trans. Antennas Propag.*, vol. 62, no. 5, pp. 2374–2381, May 2014.

[10] T. Kaufmann and C. Fumeaux, "Wearable textile half-mode substrate-integrated cavity antenna using embroidered vias," *IEEE Antennas Wireless Propag. Lett.*, vol. 12, pp. 805–808, 2013.

[11] W. Hong, B. Liu, Y. Wang, Q. Lai, H. Tang, X. X. Yin, Y. D. Dong, Y. Zhang, and K. Wu, "Half mode substrate integrated waveguide: A new guided wave structure for microwave and millimeter wave application," in *Proc. ICIMW*, Shanghai, China, Sep. 2006, p. 219.

[12] Q. Lai, C. Fumeaux, W. Hong, and R. Vahldieck, "Characterization of the propagation properties of the half-mode substrate integrated waveguide," *IEEE Trans. Microw. Theory Techn.*, vol. 57, no. 8, pp. 1996–2004, Aug. 2009.

[13] D. Ghosh, S. K. Ghosh, S. Chattopadhyay, S. Nandi, D. Chakraborty, R. Anand, R. Raj, and A. Ghosh, "Physical and quantitative analysis of compact rectangular microstrip antenna with shorted non-radiating edges for reduced cross-polarized radiation using modified cavity model," *IEEE Antennas Propag. Mag.*, vol. 56, no. 4, pp. 61–72, Aug. 2014.

[14] J.-Y. Zhang, J.-D. Zhang, W. Wu, and D.-G. Fang, "An aperture-coupled shorted-edge patch antenna with low cross polarization, adjustable beamwidth, wideband, and high gain," *IEEE Antennas Wireless Propag. Lett.*, vol. 20, pp. 2018–2022, 2021.

[15] W. An, X. Wang, H. Fu, J. Ma, X. Huang, and B. Feng, "Low-profile wideband slot-loaded patch antenna with multiresonant modes," *IEEE Antennas Wireless Propag. Lett.*, vol. 17, pp. 1309–1313, 2018.

[16] J. Wen, D. Xie, and L. Zhu, "Bandwidth-enhanced high-gain microstrip patch antenna under TM_{30} and TM_{50} dual-mode resonances," *IEEE Antennas Wireless Propag. Lett.*, vol. 18, pp. 1976–1980, 2019.

[17] N.-W. Liu, L. Zhu, and W.-W. Choi, "A low-profile wide-bandwidth planar inverted-F antenna under dual resonances: Principle and design approach," *IEEE Trans. Antennas Propag.*, vol. 65, no. 10, pp. 5019–5025, Oct. 2017.

[18] F.-X. Liu, J. Cui, J. Wang, and L. Zhao, "Textile bandwidth-enhanced half-mode substrate-integrated cavity antenna with V-slot for WLAN communications," *IEEE Antennas Wireless Propag. Lett.*, vol. 22, pp. 333–336, 2023.

[19] F.-X. Liu, J. Cui, F.-Y. Meng, T.-Y. Jiang, S.-F. Yan, S. Chao, and L. Zhao, "Textile bandwidth-enhanced polarization-reconfigurable half-mode substrate-integrated cavity antenna," *Micromachines*, vol. 14, no. 5, p. 934, Apr. 2023.

[20] J. Cui, F.-X. Liu, X. Shen, L. Zhao, and H. Yin, "Textile bandwidth-enhanced coupled-mode substrate-integrated cavity antenna with slot," *Electronics*, vol. 11, no. 15, p. 2454, Aug. 2022.

[21] N.-W. Liu, L. Zhu, G. Fu, and Y. Liu, "A low profile shorted-patch antenna with enhanced bandwidth and reduced H-plane cross-polarization," *IEEE Trans. Antennas Propag.*, vol. 66, no. 10, pp. 5602–5607, Oct. 2018.

[22] J. Cui, F.-X. Liu, H. Yin, and L. Zhao, "Textile via-loaded bandwidth-enhanced half-mode substrate-integrated cavity antenna for WLAN communications," *IEEE Trans. Antennas Propag.*, vol. 70, no. 8, pp. 6551–6559, Aug. 2022.

[23] M. H. Moradi Ardekani and H. Abiri, "A new approach to design wide band power amplifiers by compensating parasitic elements of transistors," *AEU, Int. J. Electron. Commun.*, vol. 92, pp. 1–7, Aug. 2018.

[24] M. H. M. Ardekani and H. Abiri, "A new design procedure for wide band Doherty power amplifiers," *AEU, Int. J. Electron. Commun.*, vol. 98, pp. 181–190, Jan. 2019.

[25] C. A. Balanis, *Advanced Engineering Electromagnetic*, 3rd ed., New York, NY, USA: Wiley, 2024.

MOHAMMAD HADI MORADI ARDEKANI was born in Yasouj, Iran, in 1986. He received the B.S. degree in electrical and communication engineering and the M.S. and Ph.D. degrees (Hons.) in electrical and communications engineering from Shiraz University, Shiraz, Iran, in 2009, 2012, and 2018, respectively. In 2022, he joined as an Assistant Professor with the Department of Electrical Engineering, Yasouj University, Yasouj. His research interests include the design of innovative antennas, active and passive microwave components, and electromagnetic theory and applications.

SHIMA PASHANGEH was born in Jahroom, Iran, in 1990. She received the B.S. degree in materials engineering from Yasouj University, in 2013, the M.S. degree (Hons.) in corrosion engineering from Shiraz University of Technology, in 2016, and the Ph.D. degree (Hons.) in materials engineering from Yazd University, in 2021. In 2023, she was appointed as an Assistant Professor with the Department of Materials Engineering, Yasouj University. She is currently working an accomplished Materials Engineer. Her research interests include physical metallurgy, advanced high-strength steels, corrosion science, heat treatment, composite materials, and the exploration of innovative materials.